Diffusion and geometric effects in passive advection by random arrays of vortices

M. Avellaneda and S. Torquato[a)]
Courant Institute of Mathematical Sciences, New York University, New York, New York 10012

I. C. Kim
Department of Mechanical and Aerospace Engineering, North Carolina State University, Raleigh, North Carolina 27695-7910

(Received 13 December 1990; accepted 8 April 1991)

The Lagrangian transport of a passive scalar in a class of incompressible, random stationary velocity fields, termed "random-vortex" models, is studied. These fields generally consist of random distributions of finite-sized elementary vortices in space with zero mean velocity in the presence of molecular diffusion D. The effects of vortex density, vortex strength, and sign of the vorticity on the Lagrangian history of a fluid particle [i.e., mean-square displacement $\sigma^2(t)$ and velocity autocorrelation function $\mathscr{R}(t)$] on the specific random-vortex models which possess identical energy spectra but different higher-order statistics for a Péclet number of 100 are investigated. This is done by a combination of Monte Carlo simulations of the Langevin equations and analysis. It is found that the Lagrangian autocorrelation $\mathscr{R}(t)$ and the mean-square displacement $\sigma^2(t)$ can be significantly different as the density of the vortices increases and when there are long-range correlations in the sign of the vorticity. A simple theory based on a model for $\mathscr{R}(t)$ agrees strikingly well with the present simulations. It is found that D^* increases with vortex density, suggesting that Gaussian fields are maximally dissipative among a wide class of vortex flows with given energy spectra.

I. INTRODUCTION

The problem of passive transport of a scalar in a random Eulerian velocity field has a rich history, beginning with the pioneering paper of Taylor.[1] The problem consists of studying from a statistical viewpoint the evolution of marked fluid particles advected by a prescribed random velocity field in the presence of molecular diffusion with diffusivity D. Important applications of this problem occur in flow in porous media,[2,3] Lagrangian chaos,[4] turbulent flow,[5] etc. For incompressible velocity fields (the subject of this paper), the effective diffusivity D^* is always larger than D and, in instances of convection-dominated flows, can be very large (e.g., atmospheric turbulence). Over 20 years ago, Kraichnan[6] and Saffman,[7] among others, studied various aspects of this problem. Kraichnan studied, in particular, Gaussian velocity fields, both time independent and time dependent, with prescribed energy spectra and carried out numerical experiments with $D = 0$ for such models for the first time.[6] A comprehensive survey of this passive advection problem can be found in Monin and Yaglom.[5] More recently, using the theory of multiscale expansions, or homogenization, the problem was investigated by Papanicolaou *et al.*[8] and others.[9,10]

A primary issue is to determine the Lagrangian properties of the tracer particle in terms of the given velocity statistics. In principle, this determination can be made by solving a Langevin equation for the motion of particles but, in practice, this is mathematically intractable due to the complexity of the velocity field. Much of the previous work on dispersion due to random velocity fields has concentrated on Gaussian statistics. While Gaussian statistics are important, it is of value to study transport by more realistic non-Gaussian velocity fields, given that, except in the Gaussian case, knowledge of the energy spectrum (or, equivalently, Eulerian two-point velocity statistics) is, of itself, insufficient to determine fully the velocity. In particular, velocity fields with the same energy spectrum can have completely different streamline patterns and thus the Lagrangian histories will differ.

This paper represents an initial effort in a general program of understanding dispersion in complex chaotic flows, such as those that arise in flow in porous media and Rayleigh–Bénard convection near the transition to chaos, by studying random models with a physical space description. To begin with, and for simplicity of analysis and computations, we consider "frozen" or time-independent model fields in the spirit of Kraichnan and others. Although the importance of time-independent models has been recognized in the study of "Lagrangian turbulence" for some time, heretofore there have been few random models of passive advection which have been computationally tractable.

Here we introduce a class of velocity fields that we term "random-vortex" models to study the effects of higher-order statistics on Lagrangian transport. Essentially this class of models consists of a random distribution of "elementary" vortices in space. These vortices are generally allowed to overlap, and thus by superposition of the vortex velocity fields generate complex flow patterns. Random-vortex models are a useful analytical and computational device to study

[a)] Permanent address: Department of Mechanical and Aerospace Engineering, North Carolina State University, Raleigh, North Carolina 27695-7910.

 0899-8213/91/081880-12$02.00

non-Gaussian fields. Such velocity fields serve, for instance, as models for the Darcy velocity in a porous medium containing a random distribution of momentum sources, as proposed for a related model by Koch and Brady.[3] One can thus study the effects of varying the density of vortices, vortex strength, and sign of the vorticity, while keeping the energy spectrum fixed. A wide class of energy spectra can be implemented by choosing appropriate elementary vortices.

As a first step in this direction, we study two-dimensional incompressible velocity fields containing a very simple vortex element, namely, identical vortices of finite size with solid-body rotation. For this model we are able to carry out Monte Carlo calculations of the mean square displacement $\sigma^2(t)$ of a tracer as a function of t as well as the Lagrangian autocorrelation function $\mathscr{R}(t)$ and the effective diffusivity D^* for finite but very large Péclet number Pe (Pe = 100). Since the Péclet number is finite, we know the system is diffusive, i.e., neither trapping nor superdiffusion occurs at very large times.[11] (In a future study, we will treat the case Pe = ∞ for this model.) In the computations, we vary the vortex density and orientations, while keeping the energy spectrum fixed; this results in different streamline patterns for the flows and in different Lagrangian histories. We develop a simple theory to explain these differences based on a model for the Lagrangian velocity autocorrelation function $\mathscr{R}(t)$. The theory agrees strikingly well with the simulations. The analysis proposes that the differences observed in the Lagrangian histories result from the likelihood of particles taking large advective "jumps" along relatively large "eddies" formed by the overlapping vortices.

Another interesting random model is the one proposed by Isichenko *et al.*[12] who study a superposition of stationary plane waves with randomly distributed wave vectors, as well as models based on randomly placed vortices. These authors study analytically the behavior of the effective diffusion coefficient in the limit Pe$\rightarrow\infty$ (steady-state problem), while we study primarily the Lagrangian history and D^* at finite but large Pe (dynamical problem). The study of the dependence of D^* on Pe as Pe$\rightarrow\infty$ by computational methods, albeit important, is beyond the scope of this paper.

The rest of the paper is organized as follows. In Sec. II, we briefly describe some pertinent theoretical results concerning passive advection. In Sec. III, the general class of random-vortex models is discussed and the Eulerian n-point velocity correlation functions are calculated. In Sec. IV, we describe the simulation procedure to study Lagrangian statistics. We present results for two specific random-vortex models in two dimensions: one for which all the vortices are spinning in the same direction and another where the sign of the vorticity is assigned randomly. In Sec. V, we analyze the results by proposing a simple relation between the autocorrelation function $\mathscr{R}(t)$ and distribution of eddy sizes. Finally, in Sec. VI, we make concluding remarks.

II. GENERAL THEORY

We are interested in the time evolution of scalars satisfying the advection–diffusion equation in d-dimensional space (R^d)

$$\frac{\partial C(\mathbf{x},t)}{\partial t}+\mathbf{u}(\mathbf{x})\cdot\nabla C(\mathbf{x},t)=D\nabla^2 C(x,t), \tag{1}$$

where $\mathbf{u}(\mathbf{x})$ is an incompressible, time-independent velocity field and D is a molecular dispersion coefficient. We shall assume that the velocity field $\mathbf{u}(\mathbf{x})$ is statistically homogeneous and isotropic, and satisfies

$$\nabla\cdot\mathbf{u}(\mathbf{x})=0,\qquad \langle\mathbf{u}(\mathbf{x})\rangle=0,\quad \langle|\mathbf{u}(\mathbf{x})|^2\rangle\equiv V^2<\infty. \tag{2}$$

Here angular brackets denote ensemble averaging. The scalar $C(\mathbf{x},t)$ can be thought of as representing the concentration at time t of a suspension of particles, with initial concentration $C(\mathbf{x},t=0)$, evolving according to the Langevin-type equation[5]

$$\frac{\partial\mathbf{X}(\mathbf{x},t)}{\partial t}=\mathbf{u}(\mathbf{X}(\mathbf{x},t))+\sqrt{2D}\,\mathbf{N}(t), \tag{3}$$

where $\mathbf{N}(t)$ is a d-dimensional, delta-correlated Gaussian white noise that is statistically independent of the velocity field $\mathbf{u}(\mathbf{x})$. If $C_0(\mathbf{x})=C(\mathbf{x},t=0)$ denotes the initial value of the solution of (1), this solution can be represented at later times as an expectation value (denoted by the operator $E\{\ \}$) over particle trajectories. Namely, we have

$$C(\mathbf{x},t)=\mathbf{E}\{C_0(\mathbf{X}(\mathbf{x},t))\}. \tag{4}$$

Two useful quantities in the study of the dynamics of Eqs. (1) or (3) are the *mean-square displacement*:

$$\sigma^2(t)=\langle\mathbf{E}\{|\mathbf{X}(\mathbf{x},t)|^2\}\rangle, \tag{5}$$

and the *Lagrangian velocity autocorrelation function*:

$$\mathscr{R}(t)=\langle\mathbf{E}\{\mathbf{u}(\mathbf{X}(\mathbf{x},t))\cdot\mathbf{u}(\mathbf{x})\}\rangle/\langle|\mathbf{u}(\mathbf{x})|^2\rangle. \tag{6}$$

Because $\mathbf{u}(\mathbf{x})$ is statistically homogeneous, the right-hand sides of Eqs. (5) and (6) are independent of the starting point $\mathbf{x}$, and $\sigma^2(t)$ and $\mathscr{R}(t)$ are purely functions of time. The incompressibility and unbiasedness of the field $\mathbf{u}(\mathbf{x})$ imply that (see, for instance, Monin and Yaglom[5]), for all $t>0$, $\sigma^2(t)$ and $\mathscr{R}(t)$ are related by the equation

$$\sigma^2(t)=2d\,Dt+2V^2\int_0^t(t-s)\mathscr{R}(s)ds \tag{7}$$

or,

$$\frac{d^2}{dt^2}\sigma^2(t)=2V^2\mathscr{R}(t). \tag{8}$$

The advection/diffusion of particles by a random field is in general an extremely complex process which results from advective motions along the streamlines of $\mathbf{u}(\mathbf{x})$ combined with diffusion across streamlines. At large times, the overall behavior is determined by the dynamical structure of the flow field, the dissipation, and the interplay between advection and diffusion. A standard measure of the relative effects of advection and diffusion in the long-time limit is the Péclet number, defined by

$$\mathrm{Pe}^2=\int_{R^d\setminus\{0\}}\frac{1}{D^2|\mathbf{k}|^2}\langle|d\hat{\mathbf{u}}(\mathbf{k})|^2\rangle, \tag{9}$$

where $d\hat{\mathbf{u}}(\mathbf{k})$ is the spectral measure (having dimensions of velocity) associated with the random field $\mathbf{u}(\mathbf{x})$,[5] i.e., $d\hat{\mathbf{u}}(\mathbf{k})$ is a random measure on d-dimensional space with the origin excluded (denoted by $R^d\setminus\{0\}$), such that

$$\mathbf{u}(\mathbf{x}) = \int_{R^d \setminus \{0\}} e^{i\mathbf{k}\cdot\mathbf{x}}\, d\hat{\mathbf{u}}(\mathbf{k}), \tag{10}$$

with

$$\mathbf{k}\cdot d\hat{\mathbf{u}}(\mathbf{k}) = 0, \quad \langle d\hat{\mathbf{u}}(\mathbf{k})\rangle = 0, \quad \langle d\hat{\mathbf{u}}(\mathbf{k}) \otimes d\hat{\mathbf{u}}(\mathbf{k}')\rangle = 0, \tag{11}$$

for all $\mathbf{k} \neq \mathbf{k}'$ in $R^d \setminus \{0\}$. It follows from (10) and (11) that the Eulerian two-point velocity autocorrelation function is given in terms of $d\hat{\mathbf{u}}(\mathbf{k})$, by

$$R_{\alpha\beta}(\mathbf{x}-\mathbf{y}) = \frac{\langle u_\alpha(\mathbf{x})\cdot u_\beta(\mathbf{y})\rangle}{V^2} = \frac{1}{V^2}\int_{R^d \setminus \{0\}} e^{i\mathbf{k}\cdot(\mathbf{x}-\mathbf{y})}\langle |d\hat{\mathbf{u}}(\mathbf{k})|^2\rangle, \tag{12}$$

i.e., $R(\mathbf{x})$ is the Fourier transform of the measure $\langle |d\hat{\mathbf{u}}(\mathbf{k})|^2\rangle / V^2$. Using this relation and elementary properties of the Fourier transform, it follows from (9) that

$$\mathrm{Pe}^2 = \begin{cases} \dfrac{V^2}{2\pi D^2}\displaystyle\int_{R^2} R_{\alpha\alpha}(\mathbf{x})\log|\mathbf{x}|\,d\mathbf{x}, & \text{if } d=2, \\ \dfrac{V^2}{4\pi D^2}\displaystyle\int_{R^3} \frac{R_{\alpha\alpha}(\mathbf{x})}{|\mathbf{x}|}\,d\mathbf{x}, & \text{if } d=3. \end{cases} \tag{13}$$

It has been shown by several authors[8-10] that if $\mathrm{Pe} < +\infty$, the behavior of the system for long times is diffusive, i.e., there exists D^* such that

$$\lim_{t\to\infty}[\sigma^2(t)/t] = 2dD^*. \tag{14}$$

In this paper we will be concerned only with flows for which the Péclet number (9) is finite and hence (14) holds for some D^*, the *effective diffusivity* (or dispersion coefficient) of the system. Integrating (7) by parts yields the alternative relation

$$D^* = D + \frac{V^2}{d}\int_0^{+\infty} \mathscr{R}(s)\,ds, \tag{15}$$

where the integral can easily be shown to be positive; thus we have $D^* > D$. Hence if $\mathrm{Pe} < +\infty$, the system settles into a diffusive regime at long times, in which particles evolve according to an apparently homogeneous random walk with diffusivity D^*. While at very short times we have $\sigma^2(t) = V^2t^2 + o(t^2)$, the behavior of the mean-square displacement at intermediate times is determined by the streamline patterns and the amplitude of the velocity along streamlines. For instance, if advection along closed streamlines occurs with sufficiently high probability over a certain time interval, $0 \leqslant t \leqslant t_0$ the mean-square displacement can scale with time like $\sigma^2(t) \propto t^\alpha$ with $\alpha < 1$ over this interval. The behavior of $\sigma^2(t)$ at intermediate times is, in general, determined by the fluctuations of the Lagrangian autocorrelation function $\mathscr{R}(t)$, with large fluctuations resulting in the occurrence of long transient behavior. One can obtain a coarse statistical measure of such transients by considering a formal asymptotic expansion of $\sigma^2(t)$, for large t, to the next leading order, i.e.,

$$\frac{\sigma^2(t)}{2d} = D^*t + \delta_0 + o(1), \tag{16}$$

in which

$$\delta_0 = -\frac{V^2}{d}\int_0^{+\infty} s\mathscr{R}(s)\,ds. \tag{17}$$

In general, δ_0 may not exist, i.e., the first moment of $\mathscr{R}(t)$ may diverge. For instance it is possible that

$$\frac{\sigma^2(t)}{2d} = D^*t + ct^\alpha + o(1), \tag{18}$$

where $0 < \alpha < 1$, which is a function that still satisfies Eq. (14). Nevertheless, if $\mathscr{R}(t)$ decays sufficiently fast, δ_0 will exist, in which case we refer to it as the *intercept*. This constant can be either positive or negative according to the Lagrangian properties of the flow and the size of the molecular diffusion coefficient, D. If δ_0 is positive the Lagrangian velocity autocorrelation must take appreciable negative values. This constitutes a signature of "trapping" of Lagrangian particles in closed eddies. Thus, the value of δ_0 should be influenced to some extent by the streamline structure, a point to which we shall return in the discussion of the Monte Carlo simulations.

III. RANDOM-VORTEX MODELS OF ADVECTION

A. A class of new models

The Eulerian velocity $\mathbf{u}(\mathbf{x})$, which appears in the advection–diffusion equation (1), is a prescribed stationary random field satisfying incompressibility and whose mean is zero. In two dimensions, it is useful to introduce a streamfunction $\Psi(\mathbf{x})$, defined through the relation

$$\mathbf{u}(\mathbf{x}) = \mathbf{J}\nabla\Psi(\mathbf{x}), \tag{19}$$

where

$$J = \begin{pmatrix} 0 & 1 \\ -1 & 0 \end{pmatrix}. \tag{20}$$

Combination of (1) and (8) yields, after some algebra, the relation between the Péclet number and streamfunction:

$$\mathrm{Pe}^2 = (1/D^2)[\langle\Psi^2(\mathbf{x})\rangle - \langle\Psi(\mathbf{x})\rangle^2]. \tag{21}$$

We describe here a class of *random-vortex models* of advection. For purposes of generality, consider the following two-dimensional flow fields in space $\mathbf{A}$ of area A consisting of the superposition of N identical circular "vortices" of radius a whose position $\mathbf{r}^N \equiv \{\mathbf{r}_1,\ldots,\mathbf{r}_N\}$ are distributed throughout the space $\mathbf{A}$ according to the n-body probability density function $P_N(\mathbf{r}^N)$ (defined below):

$$\Psi(\mathbf{x}) = \sum_{i=1}^{N} \epsilon_i \psi(\mathbf{x}-\mathbf{r}_i), \tag{22}$$

where ψ is the individual vortex streamfunction with compact support on the circle of radius a, i.e.,

$$\psi(|\mathbf{x}-\mathbf{r}_i|) = 0, \quad |\mathbf{x}-\mathbf{r}_i| > a, \quad \forall i, \tag{23}$$

and the random variable

$$\epsilon_i = \pm 1 \tag{24}$$

specifies the sign of the vorticity. The choice (23) implies that $\Psi(\mathbf{x}) = 0$ exterior to the space occupied by the vortices and ensures (as shall be shown below) that Ψ is continuous across the perimeter of the vortices. The velocity field corresponding to (19), (22), and (23) is then given by

$$\mathbf{u}(\mathbf{x}) = \sum_{i=1}^{N} \epsilon_i \mathbf{v}(\mathbf{x} - \mathbf{r}_i), \tag{25}$$

where the velocity associated with the ith vortex is given by

$$\mathbf{v}(\mathbf{x} - \mathbf{r}_i) = \begin{cases} \mathbf{J}\nabla\psi(\mathbf{x} - \mathbf{r}_i), & |\mathbf{x} - \mathbf{r}_i| < a, \\ 0, & |\mathbf{x} - \mathbf{r}_i| > a. \end{cases} \tag{26}$$

The overall flow field $\mathbf{u}$ (which is a superposition of the vortices) can be quite complex depending upon the topology of the clusters of vortices. We shall return to this point shortly. The class of models described above can easily be generalized to include vortices with a polydispersivity in size, i.e., characterized by a continuous size distribution. This generalization would permit the study of long-range spatial correlations in the advective field, a question that has attracted much attention in connection with the phenomena of long transients and anomalous diffusion.[13-16] It is only for simplicity and as a first step that we treat identical (monodispersed) vortices here. The case of polydispersed vortices will be the subject of a future paper. Notice also that random-vortex models are not limited to two dimensions, i.e., such models can be used to generate three-dimensional flows as well.

Using (21) and (22) we can compute an explicit expression for the Péclet number of the random-vortex model. The quantity $P_N(\mathbf{r}^N)\, d\mathbf{r}^N$ gives the probability that vortex 1 is in $d\mathbf{r}_1$ about $\mathbf{r}_1$, vortex 2 is in $d\mathbf{r}_2$ about $\mathbf{r}_2$,..., and vortex N is in $d\mathbf{r}_N$ about $\mathbf{r}_N$ and normalizes to unity. The ensemble average of any many-body function $F(\mathbf{r}^N)$ is given by

$$\langle F(\mathbf{r}^N) \rangle = \int F(\mathbf{r}^N) P_N(\mathbf{r}^N) d\mathbf{r}^N. \tag{27}$$

It is convenient to introduce the "generic" n-vortex probability density defined by

$$\rho_n(\mathbf{r}^N) = \frac{N!}{(N-n)!} \int P_N(\mathbf{r}^N) d\mathbf{r}^{N-n}, \tag{28}$$

where $d\mathbf{r}^{N-n} \equiv d\mathbf{r}_{n+1} \cdots d\mathbf{r}_N$. Here, $\rho_n(\mathbf{r}^n)$ characterizes the probability of finding any $n < N$ vortices with configuration $\mathbf{r}^n$. Since we will be considering stationary (homogeneous) random fields, it is implicit that the "thermodynamic limit" is taken, i.e., $N \to \infty$, $A \to \infty$, in such a way that $\rho = N/A$, the number density, is a fixed, finite constant. For statistically homogeneous systems, the $\rho_n(\mathbf{r}^n)$ are translationally invariant and it is convenient to introduce the n-body distribution function g_n defined by

$$g_n(\mathbf{r}_{12},...,\mathbf{r}_{1n}) = \rho_n(\mathbf{r}_{12},...,\mathbf{r}_{1n})/\rho^n, \tag{29}$$

where $\rho_1(\mathbf{r}_i) = \rho$, $\forall i$. For "fully penetrable" (i.e., spatially uncorrelated or Poisson distributed) vortices, the g_n are especially simple:

$$g_n(\mathbf{r}_{12},...,\mathbf{r}_{1n}) = 1, \quad \forall \mathbf{r}_{ij}. \tag{30}$$

For general interaction potentials between vortices, the g_n are more complex, but such situations are not considered here.

Use of (21) and (27)–(29) yields the following explicit relation for random vortex models:

$$\mathrm{Pe}^2 = \frac{1}{D^2}\Big(\rho \int \psi^2(\mathbf{x} - \mathbf{r}_1) d\mathbf{r}_1 + \rho^2 \times \int\int \overline{\epsilon_1 \epsilon_2}\, \psi(\mathbf{x} - \mathbf{r}_1)\psi(\mathbf{x} - \mathbf{r}_2) g_2(\mathbf{r}_{12}) d\mathbf{r}_1\, d\mathbf{r}_2 - \rho^2 \int \bar{\epsilon}_1 \psi(\mathbf{x} - \mathbf{r}_1) d\mathbf{r}_1 \int \bar{\epsilon}_2 \psi(\mathbf{x} - \mathbf{r}_2) d\mathbf{r}_2\Big). \tag{31}$$

Overbars over the ϵ_i indicate orientation averaging; generally such correlations are functions of position. It is thus seen that the Péclet number for this class of flow fields depends upon the vortex streamfunction, the statistics of the circulation directions, and the microgeometry of the vortices through the number density ρ and the pair correlation $g_2(\mathbf{r}_{12})$.

If the orientations of the vortices are randomly and independently distributed, (31) becomes

$$\mathrm{Pe}^2 = \frac{\rho}{D^2} \int \psi^2(\mathbf{x} - \mathbf{r}_1) d\mathbf{r}_1 = \frac{\eta}{D^2 \pi a^2} \int \psi^2(\mathbf{x} - \mathbf{r}_1) d\mathbf{r}_1, \tag{32}$$

where

$$\eta = \rho \pi a^2 \tag{33}$$

is a reduced density. Note that η is equal to the volume fraction of vortices ϕ only in the case of totally impenetrable vortices. If the vortices can overlap to any degree, then $\eta < \phi$.

If the vortices have positive orientation only, then (31) yields

$$\mathrm{Pe}^2 = \frac{1}{D^2}\Big(\rho \int \psi^2(\mathbf{x} - \mathbf{r}_1) d\mathbf{r}_1 + \rho^2 \times \int\int \psi(\mathbf{x} - \mathbf{r}_1)\psi(\mathbf{x} - \mathbf{r}_2)[g_2(\mathbf{r}_{12}) - 1] d\mathbf{r}_1\, d\mathbf{r}_2\Big). \tag{34}$$

For the case of Poisson distributed vortices, (30) holds and (34) becomes

$$\mathrm{Pe}^2 = \frac{\eta}{D^2 \pi a^2} \int \psi^2(\mathbf{x} - \mathbf{r}_1) d\mathbf{r}_1, \tag{35}$$

which is identical to the random-orientation result (32).

Let us now be more specific about the particular random-vortex model we wish to study. To begin, consider vortices with simple solid-body rotation. Letting v_θ and v_r be the tangential and radial components of $\mathbf{v}$ (with $v_r = 0$), we have

$$v_\theta(r) = \begin{cases} U_0(r/a), & r < a, \\ 0, & r > a \end{cases} \tag{36}$$

or

$$\psi(r) = \begin{cases} (U_0/2a)(r^2 - a^2), & r < a, \\ 0, & r > a. \end{cases} \tag{37}$$

Here r is a radial distance measured with respect to the vortex center. Observe that such a model possesses the peculiar feature of a discontinuous velocity at the vortex perimeter. It would have been more desirable to have chosen vortices with a smooth velocity decaying rapidly at infinity. In the present computation we have chosen vortices with compact support

as a device to keep track of the relation between the vortex density and the underlying streamline structure, which then depends on the shape and size of random clusters of vortices, a question that has been extensively studied in continuum percolation theory. Physically, any smoothly and rapidly decaying vortex has an effective finite radial extent, since the Péclet number is finite, and hence the qualitative features associated with variations of vortex density are the same whether the vortex is compactly supported or not. This similarity breaks down as $\mathrm{Pe} \to \infty$, but so does the general hydrodynamics. The discontinuity of the velocity field is mitigated by the presence of dissipation ($D \neq 0$). In our simulations (see Sec. IV), we were careful to employ a sufficiently fine space-time resolution to avoid numerical error from underresolving the motion near the vortex edges, as well as the motion within vortices. Jump discontinuities of the velocity field do not affect substantially the long-time/large-scale behavior and have been used by other authors to facilitate the calculations.[14,15]

As noted earlier, even simple vortex flows, can yield complicated flow patterns. If the vortices overlap to any degree, then the topology of the streamlines can be very complex. Owing to large-scale structures (i.e., large connected clusters of vortices), large-scale convective motions can exist, resulting in enhanced long-time transport. In this paper we shall focus our attention on two specific cases of random-vortex models that we will refer to as model I and model II. Both models consist of Poisson distributed vortices with solid-body rotation as given by (37). In model I the orientation of the vortices is randomly and independently distributed, whereas in model II all the vortices have positive orientation, say clockwise. From the discussion above it is clear that both models possess the same Péclet number given generally by (32) or (35). Substitution of (37) into either of these relations gives

$$\mathrm{Pe} = (U_0 a/2D)\sqrt{\eta/3}. \tag{38}$$

Here η [(33)] is related to the volume fraction of vortices by

$$\phi = 1 - \exp(-\eta). \tag{39}$$

In Fig. 1 we depict a realization of Poisson distributed circles at a reduced density $\eta = 0.4$ ($\phi \simeq 0.33$), which is well below the percolation-threshold value $\eta_c \simeq 1.14$.[17] The cluster sizes are not large, as expected. Although the streamline topology can already be nontrivial at this density, the streamlines will always be closed curves forming small isolated islands. Figures 2 and 3 show Poisson distributed circles at $\eta = 1.6$ ($\phi \simeq 0.8$), $\eta = 2.3$ ($\phi \simeq 0.9$), densities well above the threshold value. At such densities, the streamlines are still closed curves but their topology becomes increasingly complex as η increases.

B. Eulerian velocity correlation functions for random-vortex models

Here we obtain explicit expressions for the n-point Eulerian velocity correlation functions in terms of the vortex velocities and the n-body distribution functions g_n. We begin by considering the two-point and four-point functions and then generalize to any n.

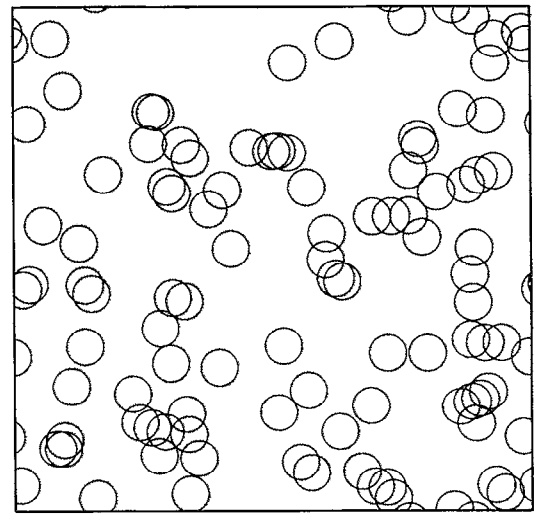

FIG. 1. A computer-generated realization of a distribution of overlapping circular vortices. Here reduced density of vortices η is 0.4, which corresponds to an area fraction ϕ of approximately 0.3.

1. Two-point correlation function

The ensemble average of the product of $\mathbf{u}(\mathbf{x}_1)$ and $\mathbf{u}(\mathbf{x}_2)$ for general random-vortex models is obtained by a combination of (25), (26), (28), and (29), with the result that

$$\langle \mathbf{u}(\mathbf{x}_1)\cdot\mathbf{u}(\mathbf{x}_2)\rangle = \rho \int \overline{\epsilon_1^2}\,\mathbf{v}(\mathbf{x}_1 - \mathbf{r}_1)\cdot\mathbf{v}(\mathbf{x}_2 - \mathbf{r}_1)\,d\mathbf{r}_1 + \rho^2 \int\int \overline{\epsilon_1\epsilon_2}\,\mathbf{v}(\mathbf{x}_1 - \mathbf{r}_1)\cdot\mathbf{v}(\mathbf{x}_2 - \mathbf{r}_2) g_2(\mathbf{r}_{12})\,d\mathbf{r}_1\,d\mathbf{r}_2$$

$$= \quad + \quad \tag{40}$$

1 2 1 2

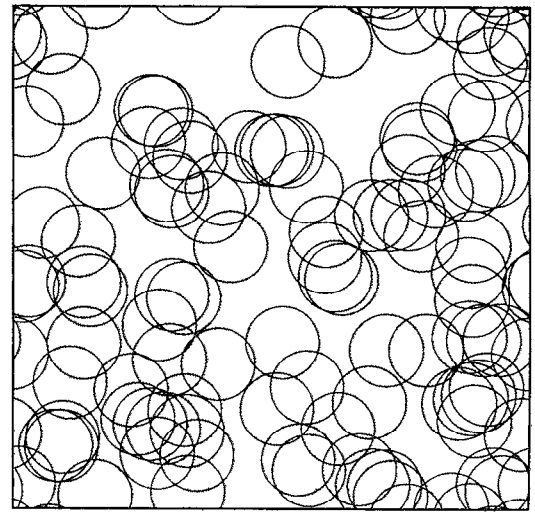

FIG. 2. A computer-generated realization of a distribution of overlapping circular vortices. Here reduced density of vortices η is 1.6, which corresponds to an area fraction ϕ of approximately 0.8.

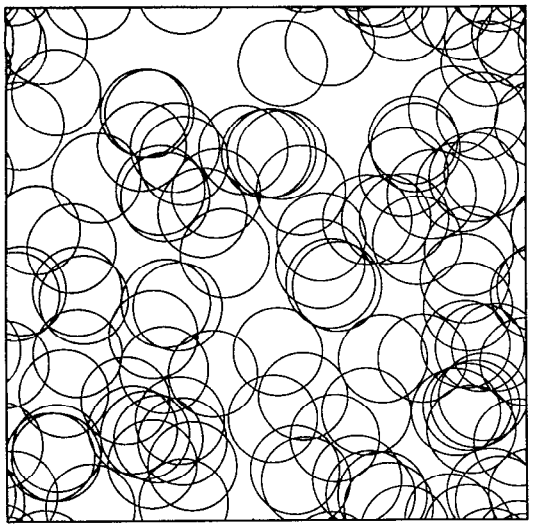

FIG. 3. A computer-generated realization of a distribution of overlapping circular vortices. Here reduced density of vortices η is 2.3, which corresponds to an area fraction ϕ of approximately 0.9.

The second line of (40) is the diagrammatic equivalent[18] of the first line. This diagrammatic notation is a compact way to indicate "cluster" integrals, especially higher-order ones.

White circles represent unintegrated positions (in this case $\mathbf{x}_1$ and $\mathbf{x}_2$), while black circles represent integration over vortex positions. Associated with each black circle is a factor of ρ. Here - - - - denotes a $\mathbf{v}$ bond and —— denotes a g_2 bond. In general, associated with each diagram is an average involving certain products of ϵ_i, i.e., orientation correlations. The orientation correlations associated with the diagrams of (40) are obvious. (Note that $\overline{\epsilon_1^2} = 1$.) A precise statement about the particular orientation correlations involved in general diagrams is given below.

Now let us consider the evaluation of (40) for the Poisson models I and II. Here $g_2 = 1$ and the two-body diagram can be written as a product of singly connected $\mathbf{v}$ bonds. Now since $\mathbf{v}$ is solid-body rotation given by (36), then $\langle \mathbf{v} \rangle = 0$ and hence for both models

$$\langle \mathbf{u}(\mathbf{x}_1)\cdot\mathbf{u}(\mathbf{x}_2)\rangle = \quad (41)$$

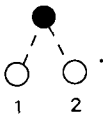

Unlike the general diagrams, the diagram of (41) does *not* involve orientation correlations. Thus the Eulerian two-point correlation function is the *same* for both models and it follows from (13) that both models have the same *Péclet number at fixed reduced density* η, a conclusion already reached using the Péclet number/streamfunction relation (21).

2. Four-point correlation function

Application of relations (25), (26), (28), and (29) yields the Eulerian four-point correlation function for the general random-vortex model to be

$$\langle \mathbf{u}(\mathbf{x}_1)\cdot\mathbf{u}(\mathbf{x}_2)\cdot\mathbf{u}(\mathbf{x}_3)\cdot\mathbf{u}(\mathbf{x}_4)\rangle =$$

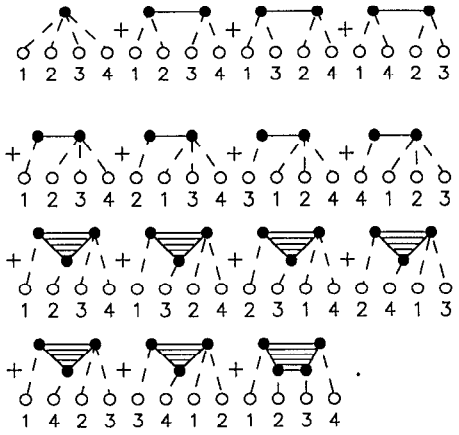

(42)

Here 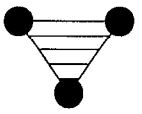

and 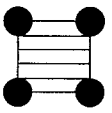

designate a g_3 bond and g_4 bond, respectively.

For models I and II, we have

$$\langle \mathbf{u}(\mathbf{x}_1)\cdot\mathbf{u}(\mathbf{x}_2)\cdot\mathbf{u}(\mathbf{x}_3)\cdot\mathbf{u}(\mathbf{x}_4)\rangle =$$

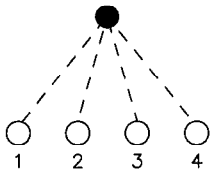

$$+ \langle \mathbf{u}(\mathbf{x}_1)\cdot\mathbf{u}(\mathbf{x}_2)\rangle\cdot\langle \mathbf{u}(\mathbf{x}_3)\cdot\mathbf{u}(\mathbf{x}_4)\rangle$$
$$+ \langle \mathbf{u}(\mathbf{x}_1)\cdot\mathbf{u}(\mathbf{x}_3)\rangle\cdot\langle \mathbf{u}(\mathbf{x}_2)\cdot\mathbf{u}(\mathbf{x}_4)\rangle$$
$$+ \langle \mathbf{u}(\mathbf{x}_1)\cdot\mathbf{u}(\mathbf{x}_4)\rangle\cdot\langle \mathbf{u}(\mathbf{x}_2)\cdot\mathbf{u}(\mathbf{x}_3)\rangle, \quad (43)$$

where $\langle \mathbf{u}(\mathbf{x}_i)\cdot\mathbf{u}(\mathbf{x}_j)\rangle$ is a term of order ρ given by (41). Therefore, *models I and II are indistinguishable at the four-point level.* As before, the one-body diagram of (43) does not carry any factor involving orientation correlations and $\mathbf{v}$ is given by the solid-body rotation (36). The first diagram in (43) is a manifestation of the fact that the fields are *non-Gaussian.*

3. n-point correlation function for any n

Here we obtain the expression for the n-point Eulerian velocity correlation in the general random-vortex model. A *simple* diagram is one in which no pairs of circles are linked by more than one bond. Let $S_n(k)$ be the sum of simple diagrams associated with the unordered partitioning of n white labels among k black circles (with corresponding $\mathbf{v}$ bonds), such that the black circles themselves are connected by a g_k bond. [For example, $S_4(1)$ is the first diagram in (42) and $S_4(2)$ is the sum of all two-body diagrams in (42).] Associated with any diagram of $S_n(k)$ is the correlation function

$\overline{\epsilon_1^{p_1}\epsilon_2^{p_2}\cdots\epsilon_k^{p_l}}$,

where p_j is the number of white labels attached to a particular black circle, $1 \leqslant j \leqslant l$, where l is the total number of sets in the partition of the white labels. [For example, the quantity $\overline{\epsilon_1\epsilon_2\epsilon_3^2}$ appears in the integrand of the integral associated with the penultimate diagram of (42).] Then the n-point correlation function is

$$\left\langle \prod_{i=1}^{n} \mathbf{u}(\mathbf{x}_i) \right\rangle = \sum_{k=1}^{n} S_n(k). \tag{44}$$

In the case of models I and II, all diagrams involving any subgraph containing a single black circle connected to only a white circle are identically zero because of Poissonian statistics and $\langle \mathbf{v} \rangle = 0$. Similarly, all odd-order n-point correlation functions are identically zero. *Although the two-point and four-point correlation functions for models I and II are the same, they are different at the six-point level.* For example, $S_6(2)$ will not be the same among these two models because model II will involve orientation correlations which, unlike model I, vanish identically. Models I and II therefore will generally possess different Lagrangian statistics, such as the mean-square displacement $\sigma^2(t)$ and the velocity autocorrelation function $\mathscr{R}(t)$.

It is important to observe, however, that the highest-order density contribution to the n-point correlation function is of the form

$$\langle \mathbf{u}(\mathbf{x}_1)\cdot\mathbf{u}(\mathbf{x}_2)\rangle\langle \mathbf{u}(\mathbf{x}_3)\cdot\mathbf{u}(\mathbf{x}_1)\rangle\cdots\langle \mathbf{u}(\mathbf{x}_{n-1})\cdot\mathbf{u}(\mathbf{x}_n)\rangle$$

(and similar terms under permutations of the labels) and hence is of order $\rho^{n/2}$. Thus, in the limit $\rho \to \infty$, the two models in fact become identical and tend to a Gaussian velocity field $\mathbf{u}(\mathbf{x})$ that is fully specified by the two-point correlation $\langle \mathbf{u}(\mathbf{x}_1)\cdot\mathbf{u}(\mathbf{x}_2)\rangle$. From these considerations we expect that at large η the effective diffusivities of models I and II should be approximately equal to the effective diffusivity of the corresponding Gaussian system with the same Eulerian statistics. However, the differences in the Lagrangian histories of models I and II are expected to be substantial even at high densities because of the markedly different streamline structures. In particular, the difference in the values of δ_0 should be significant.

IV. MONTE CARLO SIMULATION

For pure diffusion processes in random media without advection, efficient first-passage-time techniques have been recently developed to compute the mean-square displacement of a diffusion tracer.[19] Here we devise a new algorithm that enables one to obtain statistical measures along fluid particle trajectories. We present specific results for the mean-square displacement and the Lagrangian velocity autocorrelation function as functions of time.

A. Simulation procedure

Obtaining statistical measures from computer simulations is a two-step process. First, one generates realizations of the random velocity field. Second, one samples each realization for the statistical measure of interest and averages over a sufficiently large number of realizations.

We generated realizations of N Poisson distributed vortices of radius a [with solid-body rotation specified by (39)] by randomly placing the vortex centers in a square cell of area L^2. The central cell is surrounded by periodic images of itself. In model I half the vortices have clockwise orientation and the other half have counterclockwise orientation, on average. In model II, all of the vortices have clockwise direction. We examined three different values of the reduced density η: 0.4, 1.6, and 2.3. As noted in Sec. III, $\eta = 0.4$ is the only value studied below the percolation-threshold value of $\eta_c \simeq 1.14$.

In order to compute the mean-square displacement and Lagrangian autocorrelation function, one must follow fluid particles along their trajectories. The initial location $\mathbf{x}_1$ of a fluid particle is chosen randomly in the central cell. In a *small* time interval Δt, the particle will diffuse and advect to a point $\mathbf{x}_2$ so that the mean-square displacement is $|\mathbf{x}_2 - \mathbf{x}_1|^2$. The quantity $|\mathbf{x}_2 - \mathbf{x}_1|^2$ is related to the diffusion and advection process as follows: construct a *small* imaginary circle of radius δ around $\mathbf{x}_1$. Then the mean hitting time for the walker to first strike the surface of the sphere for pure diffusion is given by

$$\Delta t = \delta^2/4D. \tag{45}$$

The displacement due to advection is taken to be

$$\mathbf{X}_A = \{[\mathbf{u}(\mathbf{x}_1) + \mathbf{u}(\mathbf{x}_1 + \delta\hat{\mathbf{n}})]/2\}\Delta t \tag{46}$$

where $\hat{\mathbf{n}}$ is a unit radial vector. Thus,

$$|\mathbf{x}_2 - \mathbf{x}_1|^2 = \delta^2 + \mathbf{X}_A\cdot\mathbf{X}_A + 2\delta\hat{\mathbf{n}}\cdot\mathbf{X}_A. \tag{47}$$

Thus the total mean-square displacement $\sigma^2(t)$ (averaged over many walks and realizations) and Lagrangian velocity autocorrelation function $\mathscr{R}(t)$ after time $t = n\Delta t$ are, respectively, given as

$$\sigma^2(t) = E[\langle |\mathbf{x}_{n+1} - \mathbf{x}_1|^2 \rangle], \tag{48}$$

$$\mathscr{R}(t) = E[\langle \mathbf{u}(\mathbf{x}_{n+1})\cdot\mathbf{u}(\mathbf{x}_1)\rangle]/E[\langle \mathbf{u}(\mathbf{x}_1)|^2\rangle], \tag{49}$$

where $\mathbf{x}_{n+1}$ is the location of the random walker after the n step from its initial release. The errors involved in decomposing the coupled diffusion–advection process into distinct diffusion and advection steps will be small provided that the step size δ is taken to be sufficiently small. In this study, we tested several different values of δ and found that a value $\delta = 2.5\times10^{-3}L$ (roughly equal to 2.5×10^{-2} times a vortex diameter) yielded results accurate to within three significant figures. This is a *very high* resolution. Nonetheless, the calculation of the Lagrangian autocorrelation is difficult to determine with high precision, much more so than $\sigma^2(t)$.

In order to test the simulation method, we computed the effective diffusion coefficient D^* for a two-dimensional periodic-layered geometry with layers of thickness L oriented in the x direction. Each layer possesses an x-component velocity U which periodically alternates in sign in the y direction (i.e., the transverse direction). Our simulation results for this idealized model were in excellent agreement with the exact result for the effective diffusivity in the x direction D_{11}^*, which is easily shown to be given by

$$D_{11}^*/D = 1 + (U^2L^2/12D^2). \tag{50}$$

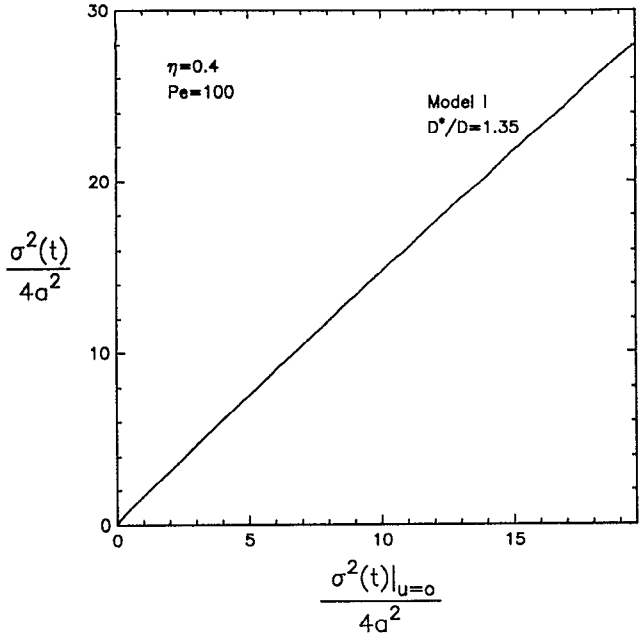

FIG. 4. Dimensionless mean-square displacement $\sigma^2(t)/4a^2$ as a function of a dimensionless time $\sigma^2(t)|_{u=0}/4a^2$ for model I at $\eta = 0.4$ and Pe = 100. The dimensionless effective diffusivity D^*/D, the slope of the tangent line of the data at largest time available $\sigma^2(t)|_{u=0}/4a^2 \sim 19.5$, is calculated to be 1.35 in this case.

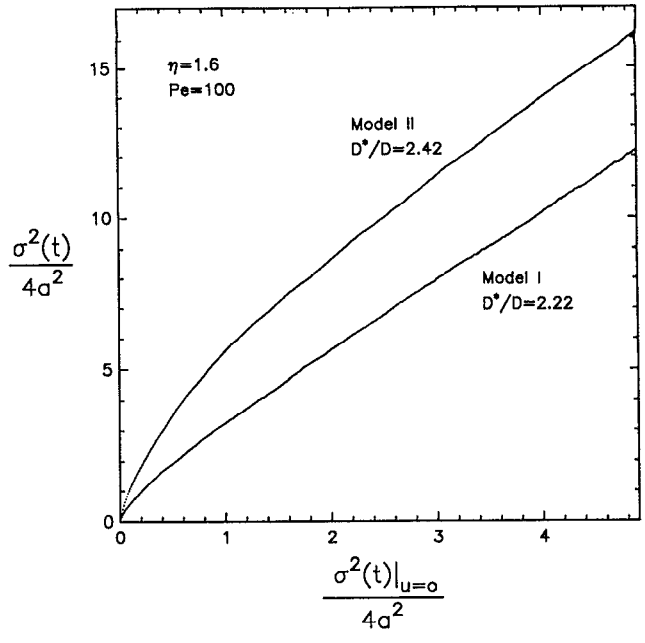

FIG. 5. Dimensionless mean-square displacements $\sigma^2(t)/4a^2$ as functions of a dimensionless time $\sigma^2(t)|_{u=0}/4a^2$ for models I and II at $\eta = 1.6$ and Pe = 100. The dimensionless effective diffusivities D^*/D, the slope of the tangent line of the data at the largest time available $\sigma^2(t)|_{u=0}/4a^2 \sim 4.9$, are calculated to be 2.22 for model I and 2.42 for model II in this case.

In our simulations for the random-vortex models, we employed $N = 100$, 1000 walks per configuration, 20–500 realizations (depending on the density of the vortices), and a Péclet number equal to 100. The value of $N = 100$ was found to be sufficiently large to neglect any system-size effects.

B. Results

We carried out long-time studies of the mean-square displacement $\sigma^2(t)$ and determined the effective diffusion coefficient D^* as defined by relation (14). Figure 4 shows for model I (random orientations) at $\eta = 0.4$ the dimensionless mean-square displacement $\sigma^2(t)/4a^2$ versus the dimensionless time

$$t^* = \frac{\sigma^2(t)}{4D}\bigg|_{u=0} \cdot \frac{D}{a^2} = \frac{\sigma^2(t)}{4a^2}\bigg|_{u=0}, \tag{51}$$

where the subscript $\mathbf{u} = 0$ indicates the mean-square displacement in the absence of advection (pure diffusion). Here $D^*/D = 1.35$ and $\delta_0/a^2 = 1.61$. These data (see Table I) are determined from the tangent line at the largest dimensionless time reported ($t^* = 19.5$). A log–log plot of the mean-square displacement versus time revealed an exponent very close to unity, indicating that $t^* = 19.5$ is sufficiently large.

In Fig. 5 we plot the mean-square displacement versus time for both models I and II at $\eta = 1.6$. For model I, $D^*/D = 2.22$ and $\delta_0/a^2 = 1.28$. For model II, $D^*/D = 2.42$

TABLE I. Data for the scaled effective diffusivity D^*/D and dimensionless maximum time t^*_{max} allowed for each random walk trajectory, where $t^* = \sigma^2(t)|_{u=0}/4a^2$.

η	Model I D^*/D	Model II D^*/D	t^*_{max}
0.4	1.35		19.5
1.6	2.22	2.42	4.9
2.3	2.26		3.5

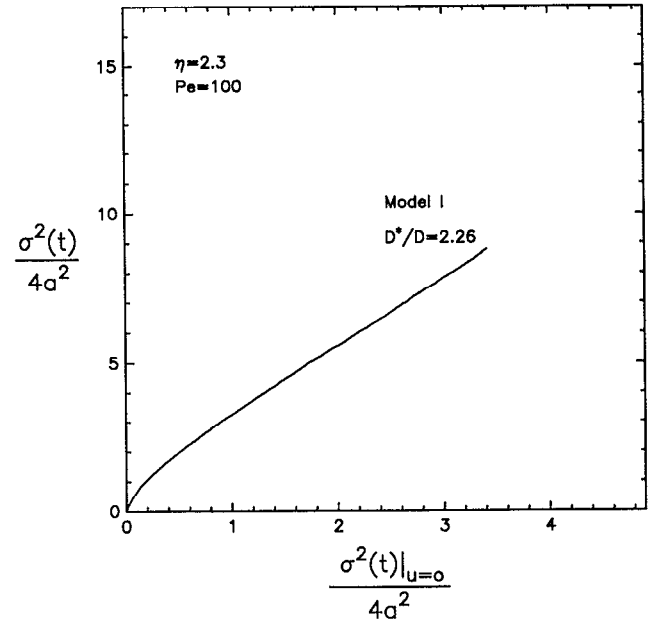

FIG. 6. Dimensionless mean-square displacement $\sigma^2(t)/4a^2$ as a function of a dimensionless time $\sigma^2(t)|_{u=0}/4a^2$ for model I at $\eta = 2.3$ and Pe = 100. The dimensionless effective diffusivity D^*/D, the slope of the tangent line of the data at largest time available $\sigma^2(t)|_{u=0}/4a^2 \sim 3.5$, is calculated to be 2.26 in this case.

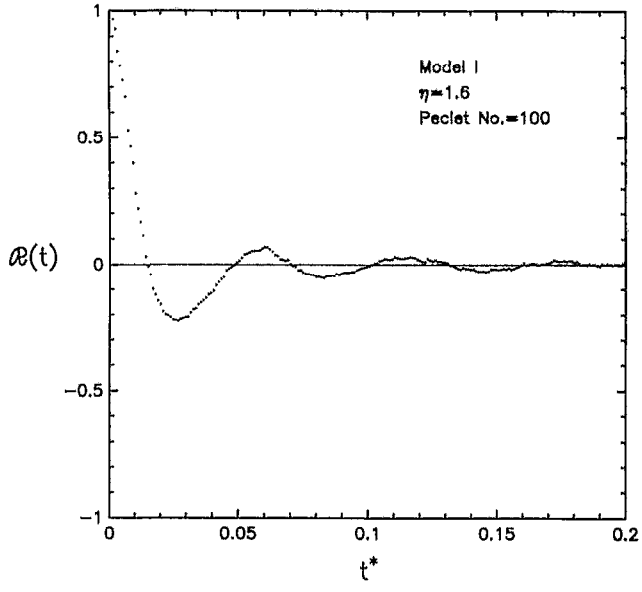

FIG. 7. Lagrangian velocity autocorrelation function $\mathscr{R}(t)$ for model I as a function of dimensionless time $t^* = \sigma^2(t)|_{u=0}/4a^2$ at $\eta = 1.6$ and $\mathrm{Pe} = 100$.

and $\delta_0/a^2 = 4.30$. These parameters were determined in the same manner as in Fig. 4. Although the maximum time reported in this figure is sufficiently large to provide reasonable estimates of D^* for both models and δ_0 for model I, the same is not true for the estimate of δ_0 for model II. Nonetheless, because of the convexity of $\sigma^2(t)$ on the scale of the figure, our estimates of D^* and δ_0, in general, are upper bounds and lower bounds, respectively, on these quantities. There are several observations worth noting here. First, as one crosses the percolation threshold from $\eta = 0.4$ to $\eta = 1.6$, the effective diffusion coefficient increases by about a factor of 2. Second, at $\eta = 1.6$, model II possesses longer transients than model I as evidenced by a larger intercept δ_0. Third, the effective diffusion coefficients for models I and II are essentially the same.

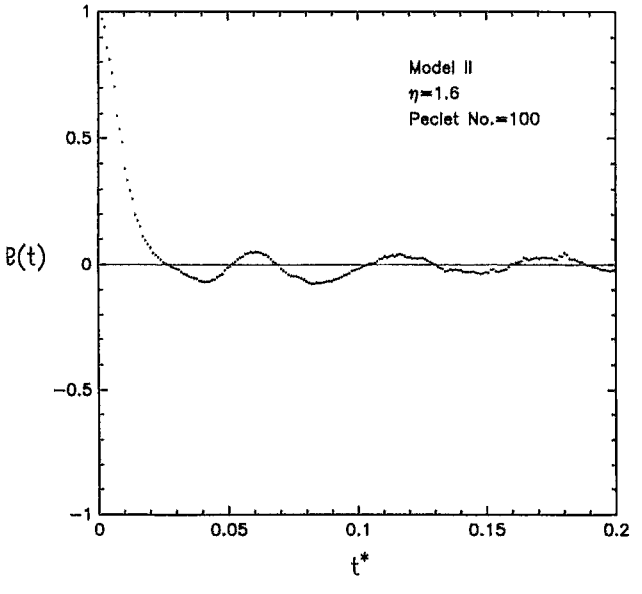

FIG. 8. As in Fig. 7, except for model II.

Figure 6 depicts the corresponding curve for model I at $\eta = 2.3$. Here $D^*/D = 2.26$ and $\delta_0/a^2 = 1.04$. Note that there is very little difference between D^* for model I at $\eta = 1.6$ and $\eta = 2.3$. Although our estimate of D^* (an upper bound) is relatively accurate, the same cannot be said of our evaluation of δ_0 here (albeit a lower bound). Nonetheless, the results obtained for δ_0 give qualitatively correct behavior.

In Fig. 7 we depict the Lagrangian velocity autocorrelation function $\mathscr{R}(t)$ for model I at $\eta = 1.6$. Figure 8 shows the corresponding quantity for model II at $\eta = 1.6$. Although the amplitudes of the oscillations decay to zero more slowly in model II than in model I, as one would expect, model I has a deeper first minimum (reflecting trapping in small eddies) and has its first zero at a smaller value of t. The significance of this behavior in $\mathscr{R}(t)$ is discussed in the following section.

The simulations were carried out on a CRAY Y-MP and all the reported calculations required about 75 CRAY hours.

V. ANALYSIS

A. Geometry of the random-vortex models and streamlines

Inspection of the simulations shows that the duration of the initial transient, in which the average mean-square displacement $\sigma^2(t)$ is nondiffusive, is approximately of the order of $5\tau_D$, where $\tau_D \simeq a^2/D$ is the diffusion time. These small transients are due to the short-range nature of the random velocities generated by superposition of vortices.

Quantitatively, this can be ascertained by considering the Eulerian two-point correlation function, which, according to (41), is given by

$$R_{\alpha\beta}(\mathbf{x}-\mathbf{y}) = \frac{\rho}{V^2}\int v_\alpha(\mathbf{x}-\mathbf{r})v_\beta(\mathbf{y}-\mathbf{r})d\mathbf{r}. \qquad (52)$$

Since $\mathbf{v}(\mathbf{x}) = 0$ for $|\mathbf{x}| > a$, this shows that $R_{\alpha\beta}(\mathbf{x}-\mathbf{y}) = 0$ for $|\mathbf{x}-\mathbf{y}| > 2a$. This implies, since $\langle \mathbf{v} \rangle = 0$, that there cannot be, typically, large-scale motions of marked particles due to advective motion alone, irrespective of the value of the reduced density of eddies, η. Thus, if we take the "hopping" length associated with diffusion to different "eddies" (see discussion below) to be of the order of a, then the transients should occur over times of order a^2/D. We remark that the situation would be different if the vortex radii were distributed according to a long-tailed probability density; in such cases, large transients associated with strong convective effects would be observed. We do not rule out, in general, the possibility that short-range velocity correlations can give rise, through cooperative effects, to long transients, but this is definitely not the case for models I and II.

The differences between the flows at different values of η and between models I and II can be explained by examining the streamline patterns. For flows having long streamlines, or more precisely, long "channels" of streamlines, par-

ticles can be advected along such channels for intervals on the order of the diffusion time a^2/D, and then diffuse into another such channel for another period of time, etc. Because of the large Péclet number, the velocity along such channels results in the particle evolving according to a random walk with large steps, relatively to a homogeneous diffusion with variance $2D$. Thus, discrepancies in the value of η and in passing from model I to model II can influence the particle transport. Notice that model I has typical configurations consisting of small "islands" of short streamlines for densities below the percolation threshold, while much longer but finite streamlines can form with finite probability above the threshold. A substantial difference exists between models I and II above the threshold because the streamfunctions of model I oscillate more rapidly than those of model II due to the randomness of the ϵ_i, and hence lead to shorter streamlines.

B. Representation of the Lagrangian velocity correlation in terms of an eddy-frequency distribution

The enhancement in the long-time diffusivity due to the random field is given from (15) by

$$\frac{V^2}{2}\int_0^\infty \mathscr{R}(s)ds, \tag{53}$$

where the integral $\int_0^\infty \mathscr{R}(s)ds$ can be interpreted as a mean relaxation time of advective motions. In this subsection, we propose a simple picture of the Lagrangian transport from which we obtain approximate formulas for $\mathscr{R}(t)$, based on the particles alternating between successive, short convective motions, and diffusing from one channel of streamlines to another. Such channels will be referred to, for simplicity, as "eddies." Thus, by an eddy we mean a "channel" or "ribbon" formed by parallel closed streamlines for which the velocity has approximately the same magnitude. The basic approximation that is made here consists in assuming that a Lagrangian particle becomes essentially uncorrelated as the particle exits the eddy, and that this happens, on average, after a few diffusion times $\tau_D = a^2/D$. We can then argue that the autocorrelation function can be computed by averaging the contributions to $E\{\mathbf{u}(\mathbf{X}(t))\mathbf{u}(\mathbf{X}(0))\}$ arising from particles starting on different eddies over the eddy-frequency distribution.

The simplest kind of eddy that can be found in a random-vortex configuration is an isolated vortex. If we assume first that the molecular diffusion D is zero, the particle paths (for a vortex centered at $\mathbf{x}=0$) consist simply of periodic circular motions with constant angular velocity:

$$\begin{aligned} x(t) &= x(0)\cos(U_0 t/a) - y(0)\sin(U_0 t/a), \\ y(t) &= x(0)\sin(U_0 t/a) + y(0)\cos(U_0 t/a), \end{aligned} \tag{54}$$

where $(x(0), y(0))$ are the coordinates of the starting point. To compute the contribution to the velocity autocorrelation, we form the inner product

$$\begin{aligned} &\mathbf{v}(x(t),y(t))\cdot\mathbf{v}(x(0),y(0)) \\ &= (U_0^2/a^2)[(x(0))^2 + (y(0))^2]\cos(U_0 t/a) \end{aligned} \tag{55}$$

and average this function over the initial position of the particle. In this way, we obtain the purely oscillatory function

$$\mathscr{R}_{\mathbf{v}}(t)|_{D=0} = \cos(U_0 t/a), \tag{56}$$

which we interpret as the contribution to the autocorrelation arising from isolated vortices with $D=0$. Given an arbitrary eddy, or closed channel of streamlines, and assuming that $D=0$, the corresponding conditional Lagrangian velocity correlation function, given that the particle starts inside the eddy, is a periodic function

$$\mathscr{R}_{\text{cond}}(t)|_{D=0} = \sum_{k=1}^{\infty} f_k \cos k\omega t, \tag{57}$$

where f_k is a sequence of non-negative numbers such that $\Sigma_k f_k = 1$, and ω is the "fundamental frequency" corresponding to periodic motions of particles around the eddy. The fundamental frequency ω satisfies, from dimensional analysis,

$$\omega \simeq U_e/l_e, \tag{58}$$

where U_e is the velocity amplitude on the eddy and l_e is the length of a typical streamline within the eddy.

To incorporate corrections to (57) arising from a nonvanishing molecular diffusion, we make the assumption that the velocity of a particle becomes uncorrelated with the initial velocity once the particle exits the eddy (by molecular diffusion) for the first time. This assumption is made for mathematical convenience; it is nevertheless consistent with the observed simulations which exhibit damping of the nondiffusive effects after a period on the order of $\tau_D \simeq a^2/D$. This leads to an approximate expression for the conditional velocity autocorrelation given that the particle starts from a genreal eddy

$$\mathscr{R}_{\text{cond}}(t) = e^{-\omega_D t}\mathscr{R}_{\text{cond}}(t)|_{D=0}, \tag{59}$$

where $\omega_D \simeq D/a^2$ is the diffusion frequency. Equation (59) is consistent with the fact that the "width" of a typical eddy, i.e., the length scale for which the velocity fluctuations are small, is of the order of a few particle diameters. The contribution of a given eddy, with conditional correlation function (59), to the overall autocorrelation function should be given by (59) multiplied by a suitable statistical weight. Taking the average over all possible eddies and using (59), we arrive at the simple empirical formula

$$\mathscr{R}(t) \simeq e^{-\omega_D t}\int_0^\infty \cos\omega t\, f(\omega)d\omega, \tag{60}$$

where $f(\omega)$ represents a distribution of eddy frequencies. In practice, the use of this last equation is limited by the fact that such a distribution can be obtained only in a qualitative fashion. However, based on direct inspection of the vortex configurations, we know the following.

For $\eta = 0.4$ in model I, the eddies are approximately isolated vortices, so $f(\omega)$ should be strongly concentrated in a neighborhood of $\omega_e \simeq V/a$, where $V = \sqrt{\langle|u(0)|^2\rangle}$ is the typical velocity.

For $\eta = 1.6$ or 2.3 in model I, we expect a more widely dispersed eddy-frequency distribution, with range $\omega_D < \omega < \omega_e$, concentrated below ω_e.

For $\eta = 1.6$ in model II, one expects an even wider distribution of eddy frequencies, with the distribution $f(\omega)$

more weighted toward lower frequencies than in the other three flows.

It is natural to assume that, due to the short-range correlations of the velocity, and the other assumptions made in the derivation of (60), the range of active frequencies is essentially contained in the interval $\omega_D \leqslant \omega \leqslant \omega_e$.

Using the approximation (60) we consider the formulas for the implied effective diffusivity D^* and intercept δ_0, obtained from (15) and (17). We obtain, accordingly,

$$D^* = D + \frac{V^2}{2}\int_{\omega_D}^{\omega_e} \frac{\omega_D}{\omega_D^2 + \omega^2} f(\omega)\, d\omega \tag{61}$$

and

$$\delta_0 = \frac{V^2}{2}\int_{\omega_D}^{\omega_e} \frac{\omega^2 - \omega_D^2}{(\omega^2 + \omega_D^2)^2} f(\omega)\, d\omega. \tag{62}$$

These formulas bear a close resemblance to the rigorous representation of D^* and δ_0 in terms of integrals over the energy spectrum of the random Hamiltonian $\mathscr{H} = -D\nabla^2 + u(\mathbf{x})\cdot\nabla$ (see Ref. 20, for example). In fact, they correspond to the simple approximation in which the spectrum of $\mathscr{H}$ consists of the number $E_1 + iE_2 = \omega_D \pm i\omega$, with ω distributed according to the density $f(\omega)$. From (61), it is clear that the formation of large eddies above the percolation threshold and the long-range correlations in the sign of the vorticity, translate into the dispersion of eddy frequencies, and hence into enhancement of D^*. This result is supported by the physical intuition of particles performing large "jumps" by advection through eddies. From a spectral viewpoint, eigenvalues with $E_1/E_2 \gg 1$ correspond to "dissipative" states, whereas eigenvalues with $E_1/E_2 \ll 1$ correspond to "convective" states. A positive intercept δ_0 is associated with the predominance of modes for which $E_2 > E_1$ in the spectrum of $\mathscr{H}$. Our empirical formula (62) reflects this, and shows why in the random-vortex models the intercept δ_0 is always positive. The function $(\omega^2 - \omega_D^2)/(\omega^2 + \omega_D^2)^2$ appearing in (62) attains a maximum at $\omega = \omega_D\sqrt{3}$, which explains why the value of the intercept increases as the eddy-frequency distribution shifts away from a sharp peak at ω_e ($\omega_e \simeq V/a \gg \omega_D$). A positive value of δ_0 is a result of significant negative autocorrelations due to particles gyrating rapidly along eddies of different sizes. An idea of the effects of dispersion in the eddy-frequency distribution can be obtained by substituting for $f(\omega)$ the "step" functions

$$f_{\omega_0}(\omega) = [1/(\omega_e - \omega_0)]\,\mathscr{X}(\omega), \tag{63}$$

where ω_0 lies between ω_D and ω_e and where $\mathscr{X}(\omega)$ is the characteristic function of the interval $\omega_0 \leqslant \omega \leqslant \omega_e$. Substitution of (63) in (60) yields the function

$$\mathscr{R}_{\omega_0}(t) = \frac{2e^{-\omega_D t}}{t(\omega_e - \omega_0)} \sin\left(\frac{(\omega_e - \omega_0)t}{2}\right) \times \cos\left(\frac{(\omega_e + \omega_0)t}{2}\right), \tag{64}$$

which oscillates rapidly and decays in time. For instance, at $t = 1/\omega_D$ we have, for $\omega_0 \ll \omega_e$, $|\mathscr{R}_{\omega_0}(1/\omega_D)| \leqslant 2e^{-1}\omega_D/(\omega_e - \omega_0)$. In general, *dispersion in eddy frequency, results in damped, rapid oscillations of the autocorrelation function $\mathscr{R}(t)$ which enhance D^* and δ_0.*

Finally, it is natural to define the cutoff frequencies ω_D, and ω_e so that

$$V^2/D\omega_D = \omega_e^2/\omega_D^2 = \mathrm{Pe}^2, \tag{65}$$

and (61) can be recast as

$$\frac{D^*}{D} = 1 + \frac{1}{2}\int_0^\infty \frac{\mathrm{Pe}^2\, g(s)\, ds}{1 + \mathrm{Pe}^2\, s^2}, \tag{66}$$

with $g(s) = \omega_e f(\omega_e s)$. This establishes a connection between the eddy-frequency distribution and the Stieltjes representation measure derived in Ref. 6. Certain Padé approximants of Stieltjes functions are rigorous upper and lower bounds on such functions.[9] For example, the [1,1] Padé approximant is a lower bound. At low densities, the frequency distribution is strongly peaked near the maximum eddy frequency ω_e and hence $g(s) \simeq \delta(s - s_0)$, with $s_0 \simeq 1$. This yields the approximate expression $D^*/D = 1 + (\frac{1}{2})[\mathrm{Pe}^2/(1 + s_0\,\mathrm{Pe}^2)]$, which has the form of a [1,1] Padé approximant to (5.16), i.e., a lower bound on D^*/D. Substitution of $\mathrm{Pe} = 100$ and $s_0 = 1$ yields $D^*/D = 1.5$, which is in reasonable agreement with $D^*/D = 1.35$ for $\eta = 0.4$. Therefore, dilute arrays of random vortices give examples of flows realizing approximately the lower bound ([1,1] Padé approximant) for D^*, supplementing the very idealized models which realized such bound, studied by Avellaneda and Majda.[9]

VI. CONCLUSIONS

We have analyzed the dispersion of a passive scalar in non-Gaussian, random, incompressible velocity fields formed by aggregates of random vortices. The behavior of the mean-square displacement $\sigma^2(t)$, the Lagrangian velocity autocorrelation $\mathscr{R}(t)$, and the effective diffusivity D^* were studied as the vortex density and the vortex orientations were varied, while keeping the energy spectrum and the Péclet number fixed (at a value of 100). The main conclusions that follow from the numerical simulations and the analysis are listed below.

(i) The effective diffusivity D^* increases with the vortex density.

(ii) The effective diffusivities for models I and II at high densities are roughly equal. This conclusion agrees with the fact that as the vortex density increases, the velocities of models I and II converge in distribution to a Gaussian field with specified covariance, and therefore, in principle, the effective diffusivities should be near the Gaussian value. The computations give an idea of the fluctuations in the value of D^* arising from non-Gaussian statistics.

(iii) The Lagrangian mean-square displacement functions $\sigma^2(t)$ are increasingly downward convex as the density of the vortices increases and as the vortex orientations are correlated, reflecting the differences in the models' streamline structures. By a simple argument, we relate the streamline structure to the Lagrangian history, through a model for the Lagrangian velocity autocorrelation function. This argument explains qualitatively the differences observed herein.

(iv) We simulate the Lagrangian velocity autocorrelation functions for the models above the percolation threshold and obtain rapidly damped, oscillatory functions. The

main features of these functions are explained by our analysis.

Based on item (i) above and on the observation of the numerical simulations (see Table I), we conjecture that *Gaussian flows maximize the effective diffusivity D^* among the class of random vortex flows with the same two-point correlation function*. The investigation of this conjecture is left to a future work.

ACKNOWLEDGMENTS

The authors are thankful to the anonymous referees for their critical and useful remarks.

S. T. and I. K. gratefully acknowledge the partial support of the Office of Basic Energy Sciences, U.S. Department of Energy, under Grant No. DE-FG05-86ER13842. M. A. and S. T. acknowledge the partial support of U.S. Air Force Grant No. AFOSR-90-0090. M. A. also acknowledges support from the U.S. Army (ARO-DAAL03089-KJ-0039) and the U.S. National Science Foundation (NSF-DMS-90-05799). Some computer resources (CRAY Y-MP) were supplied by the North Carolina Supercomputing Center funded by the State of North Carolina.

[1] G. I. Taylor, Proc. London Math. Soc. Ser. 2 **20**, 196 (1921).
[2] J. A. Aronovitz and D. R. Nelson, Phys. Rev. A **30**, 1948 (1984).
[3] D. L. Koch and J. F. Brady, Phys. Fluids A **1**, 49 (1989).
[4] S. Childress, Phys. Earth Planetary Inter. **20**, 1726 (1979).
[5] A. S. Monin and A. M. Yaglom, *Statistical Fluid Mechanics: Mechanics of Turbulence*, (MIT Press, Cambridge, MA, 1971), Vols. 1 and 2.
[6] R. Kraichnan, Phys. Fluids **6**, 575 (1965).
[7] P. G. Saffman, J. Fluid Mech. **8**, 273 (1960); Phys. Fluids **12**, 1786 (1969).
[8] G. Papanicolaou, D. McLaughlin, and O. Pironneau, SIAM J. Appl. Math. **45**, 780 (1985).
[9] M. Avellaneda and A. J. Majda, Phys. Rev. Lett. **62**, 753 (1989); Commun. Math. Phys. (in press).
[10] K. Oelschlager, Ann. Prob. **16**, 1084 (1988).
[11] The square of the Péclet number [according to definition (9) or (13)] is inversely proportional to D^2 multiplied by an integral involving the energy spectrum. It was shown in Refs. 8–10 that, according to its definition, if $\mathrm{Pe} < +\infty$, then normal diffusion necessarily occurs at long times. The Péclet number can be infinite either by taking $D = 0$ or by virtue of an energy spectrum which results in a divergent integral. Since the energy spectrum in our "random-vortex" models vanishes sufficiently fast for wave numbers approaching zero, then for nonzero D, $\mathrm{Pe} < +\infty$. This is in contrast to the two-dimensional study of Aronovitz and Nelson (Ref. 2) who consider a flat spectrum (i.e., white noise spectrum) near $k = 0$ and thus always obtain anomalous diffusion, regardless of the value of the diffusion coefficient. Thus, depending on the class of spectra one examines, diffusion can either be normal or anomalous at long times when $D \neq 0$, irrespective of the space dimension.
[12] M. B. Isichenko, J. L. Kalda, E. B. Tatarinova, O. V. Tel'kovskaya, and V. V. Yankov, Sov. Phys. JETP **69**, 517 (1989).
[13] G. Matheron and G. DeMarsily, Water Resour. Res. **16**, 901 (1980).
[14] J. P. Bouchaud, A. Comptet, A. Georges, and P. Le Doussal, J. Phys. (Paris) **48**, 1445 (1987).
[15] J. P. Bouchaud, A. Georges, J. Koplik, A. Provata, and S. Redner, Phys. Rev. Lett. **64**, 2503 (1990).
[16] M. Avellaneda and A. J. Majda, Commun. Math. Phys. **131**, 381 (1990).
[17] S. W. Haan and R. Zwanzig, J. Phys. A **10**, 1547 (1977); E. T. Gawlinski and H. E. Stanley, *ibid.* **14**, L291 (1981); S. B. Lee and S. Torquato, Phys. Rev. A **41**, 5338 (1990).
[18] J. P. Hansen and I. R. McDonald, *Theory of Simple Liquids* (Academic, New York, 1986).
[19] S. Torquato and I. C. Kim, Appl. Phys. Lett. **55**, 1847 (1989); I. C. Kim and S. Torquato, J. Appl. Phys. **68**, 3892 (1990).
[20] I. M. Lifschitz, S. A. Gredeskul, and L. A. Pastur, *Introduction to the Theory of Disordered Systems* (Wiley–Interscience, New York, 1988); R. Kubo, J. Math. Phys. **4**, 174 (1963).